Design and control of 3-DOF needle positioner for MRI-guided laser ablation of liver tumours

E. Franco*, M. Aurisicchio, M. Ristic
Mechanical Engineering Department, Imperial College London
London, UK
E-mail: ef1311@imperial.ac.uk
E-mail: m.ristic@imperial.ac.uk
*Corresponding author

Abstract: This article presents the design and control of a pneumatic needle positioner for laser ablation of liver tumours under guidance by Magnetic Resonance Imaging (MRI). The prototype was developed to provide accurate point-to-point remote positioning of a needle guide inside an MR scanner with the aim of evaluating the potential advantages over the manual procedure. In order to minimize alterations to the MR environment the system employs plastic pneumatic actuators and 9 m long supply lines connecting with the control hardware located outside the magnet room. An improved Sliding Mode Control (SMC) scheme was designed for the position control of the device. Wireless micro-coil fiducials are used for automatic registration in the reference frame of the MR scanner. The MRI-compatibility and the accuracy of the prototype are demonstrated with experiments in the MR scanner.

Keywords: Medical Robotics; Pneumatic Systems; MRI; Sliding Mode Control

Biographical notes: Enrico Franco received Bachelor and M.Sc. in Mechanical Engineering from Politecnico di Torino, Turin, Italy and the PhD degree in Medical Robotics at Imperial College, London, UK. His research interests include medical and rehabilitation robotics, nonlinear control, and mechatronics.

Marco Aurisicchio is Lecturer in the Department of Mechanical Engineering at Imperial College, London and a Senior Tutor in the Innovation Design Engineering Programme at the Royal College of Art, London UK. Prior to joining Imperial College, Marco was a Research Associate at the University of Cambridge, where he also undertook his PhD in engineering design. His research interests include the design process of complex systems and knowledge management in product development.

Mike Ristic is Senior Lecturer in the Department of Mechanical Engineering at Imperial College, London, UK. He graduated from University College London in 1981 in Mechanical Engineering. He received M.Sc. in Control Systems in 1982 and Ph.D. in Robotics in 1986, both from Imperial College London. His research interests include MRI systems integration, MRI magnets, superconducting magnets, MRI guided interventions.

This article is a revised and expanded version of the paper entitled 'Design and control of a needle positioner for MRI-guided laser ablation of the liver', presented at the International Conference on Mechatronics and Embedded Systems and Applications (MESA), MESA 2014, Senigallia, 10-12 September 2014.

1. INTRODUCTION

Laser Interstitial Thermoablation (LITT) is used to treat otherwise inoperable liver tumours by delivering thermal energy from a high power laser through a catheter probe directly to the target lesions. The lesions normally treated vary in diameter from 10 mm to 50 mm and can be located in any part of the liver (Gough-Palmer and Gedroyc, 2008). Compared to ultrasound guidance the MRI-guided procedure offers better soft tissue contrast and provides the ability to monitor the tissue temperature rise and to control the therapy delivery (Dick *et al*, 2002). During MRI-guided procedures the patient is anaesthetized and lays supine with an MR receiver coil on his abdomen. Open MR magnets have been used in this context to target the lesions with a coaxial puncture needle and to undertake thermal monitoring (Vogl *et al*, 1995). However the lower field and gradient strength of this type of scanners limit their imaging capability and speed. Cylindrical magnet MR scanners are commonly available in most hospitals, but the patient access is severely restricted. Consequently it is usual to have the catheter probe placed under ultrasound guidance at a different site in the department and to move then the patient to the MR scanner (Gedroyc, 2005). This approach results in a more complex and time consuming workflow. Moving the patient after the

catheter insertion also bears the risk of dislodging the catheter probe compromising targeting accuracy.

The aim of this research is the development of an actuated mechatronic needle positioner that will allow accurate alignment of a suitable needle guide while the patient is in the MR scanner and will assist manual needle insertion outside the bore with the goal of reducing procedure duration and improving targeting accuracy. This paper presents the design, control and validation of a first prototype with 3 degrees-of-freedom (DOF), low pressure pneumatic actuation and long supply lines.

A needle-guiding robot for microwave thermotherapy of liver tumours is presented in (Hata, Hashimoto and Tokuda, 2005). The robot has 3 actuated DOF and was designed for use in an open MR scanner. The actuation employs ultrasonic motors which resulted in noticeable image degradation when activated inside the MR scanner. Recently pneumatic actuation has been chosen for several MRI-compatible robotic devices because it produces minimum alterations to the MR environment. A 4-DOF robot for transperineal prostate biopsy with pneumatic actuation and 5 m supply lines is presented in (Song et al, 2010). A 6-DOF MRI-compatible robot actuated by special low-friction pneumatic cylinders with the control unit residing in the MRI scanner room is described in (Melzer et al, 2008). A 4-DOF parallel robot for breast biopsy actuated by pneumatic cylinders with long supply lines is described in (Yang et al, 2011a). In spite of keeping the control unit outside the scanner room operating the device in the bore led to noticeable SNR reduction due to metallic parts in the pneumatic cylinders and to the piezo motor used to actuate the needle insertion.

The prototype presented in this paper is actuated by commercially available plastic pneumatic cylinders. The use of low actuating pressure enhances safety and reduces air consumption. In order to minimize alterations to the MR environment all control hardware including the pneumatic valves is kept outside the magnet room thanks to the use of 9 m long supply lines. Position errors below 1 mm were achieved in (Yang et al, 2011b) for a similar pneumatic system using Sliding Mode Control (SMC) schemes. This paper presents an improved SMC scheme that achieved
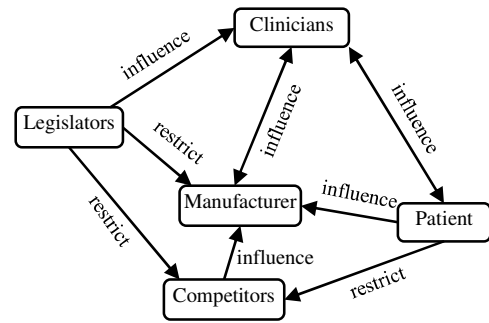

Fig. 1. Stakeholder Influence Map for the needle positioner.

steady-state position errors below 0.15 mm while resulting in lower overshoot, shorter settling time and higher tracking accuracy compared to a standard SMC design. In order to enhance the targeting accuracy of the needle positioner wireless micro-coil fiducials attached to the needle guide are used for initial registration in the MR scanner. The position of the fiducials is calculated with a tracking algorithm that provides sub-millimetre accuracy (Galassi et al, 2014).

In Section 2 of this article the design requirements for the needle guiding robot are presented and analysed. Section 3 outlines the system design. Section 4 presents the controller design. Section 5 describes the micro-coil fiducials and gives an overview of the tracking algorithm. Section 6 reports experimental results and Section 7 contains the conclusions.

2. SYSTEM REQUIREMENTS

The needle positioner is intended to operate in the MR environment and to assist clinicians in laser ablations of liver tumours. According to the definition presented in (WHO, 2003) the system falls in the category of medical devices. The system requirements were identified and analysed through a systems engineering approach involving the application of multiple methods. In particular we employed a Stakeholder Influence Map, a Viewpoint Analysis, a Systemic Textual Analysis and a Quality Functional Deployment. Although each of these methods can be regarded as a different analytical tool, these were applied in sequence for the purpose of producing a complete set of requirements. The methods were implemented using a
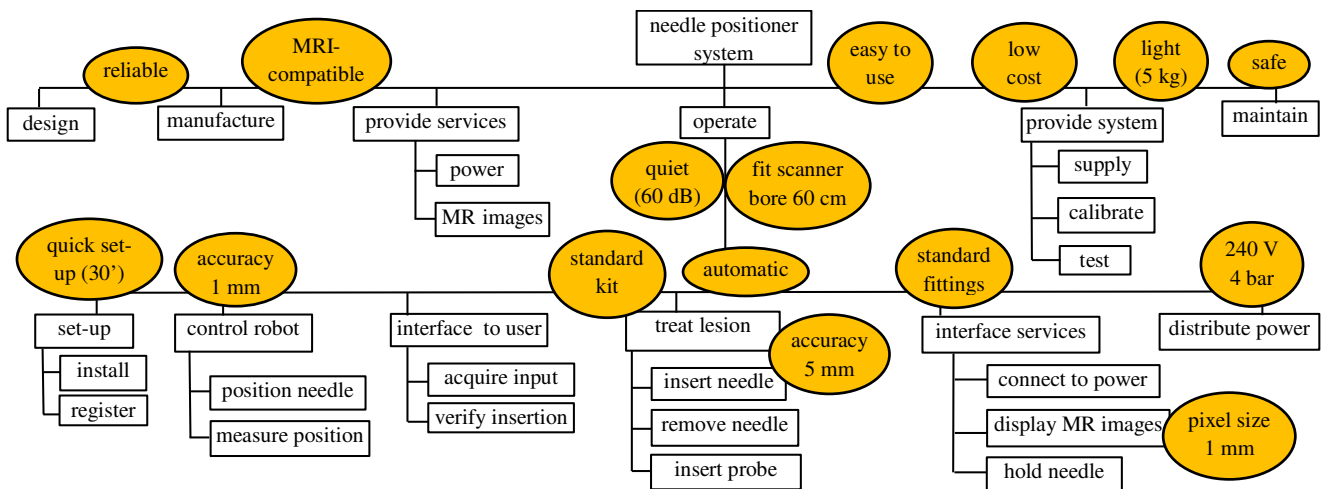

Fig. 2. Viewpoint Structured Chart for the needle positioner

Non-functional System Requirements

- light: weight < 5 kg
- quiet: noise < 60 dB
- reliable
- low cost
- MRI compatibility: ASTM F2503
- safe: Machinery, Low Voltage Directive 2006/42/EC, 2006/95/EC
- fits in the scanner: 60 cm bore
- easy to use: minimal training required

Non-Functional Implementation Requirements	Functional Requirements	Non-Functional Performance Requirements
	install device	set-up time < 30 min
	register device in the MR scanner frame	accuracy* < 1 mm
	position needle	accuracy < 1 mm; workspace* 210x160mm on coronal (xz) plane
	measure position	
	acquire user input	accuracy* < 1 mm
	verify needle insertion	
standard ablation kit (coaxial needle and catheter probe)	insert needle	accuracy < 5mm; direction inclined on axial (xy) and sagittal (zy) planes*
	remove needle	
	insert ablation probe	
	hold needle	1.2 mm*
	connect to power	standard fittings, 240 V AC, 4 bar
	distribute power	
	display MR images	pixel size 1mm

Functional requirement	Performance indicator	Verification		
		Method	Acceptance	Model
install device	set-up time	bench test	30 min	prototype
register device	accuracy	scanner test	1 mm	prototype
position needle	accuracy	scanner test	1 mm	prototype
measure position				
position needle	workspace	simulation	210x160mm on coronal plane	kinematics
measure position				
acquire input	accuracy	bench test	1 mm	user interface
verify insertion	accuracy	scanner test	1 mm	prototype
insert needle	accuracy	scanner test	5 mm accuracy	prototype
remove needle				
insert probe				
insert needle	needle movements	simulation	inclinations on axial and sagittal planes	kinematics
remove needle				
insert probe				
hold needle	diameter	simulation	1.2 mm	CAD model
connect to power	standard fittings; 240V AC, 4 bar	inspection	pass/fail	component specifications
distribute power				
display MR images	resolution	bench test	1 mm	user interface

common requirements model which distinguishes them in: 1) operational (i.e. describing the main purpose of the system with its key constraints); 2) functional (i.e. describing a function); 3) non-functional (i.e. quantifying a function's outcome or a system property). The latter were further subdivided into: 1) non-functional performance requirements (i.e. outcome of a function); 2) non-functional system requirements (i.e. constraints affecting the whole system, such as size and weight); 3) non-functional implementation requirements (i.e. imposed solutions for a specific function). In this article we present only a selection of the methods applied to provide an overview of the approach adopted and to illustrate the outcome of the requirements analysis.

The Stakeholder Influence Map (Burge, 2007) was constructed to identify the critical stakeholders at the beginning of the design process. According to this approach a list of potential stakeholders was created, five groups were formed considering subjects and entities with similar views, and a map was constructed which highlights the influences between the groups (Fig. 1). The group 'Legislators' for instance refers to norms related to machinery as well as to the MR environment, while the group 'Manufacturer' includes R&D engineers, designers, and technicians. Finally it was decided not to collect requirements from patients initially, since the procedure is normally carried out under general anaesthesia.

The operational requirements were defined in close collaboration with radiologists and MRI physicists, which are part of the group 'Clinicians'. The system is intended to be used inside a high-field closed-bore MR scanner and is required to: 1) plan and execute needle insertions quickly and accurately; 2) provide visual verification on the MR images prior to the needle insertion; 3) achieve a targeting accuracy sufficient for clinically relevant lesions; 4) target lesions within the whole liver. Additionally the system should operate with a standard ablation kit consisting of a coaxial needle and of a catheter probe (Somatex, Germany).

In order to gain a deeper understanding of the problem, additional requirements were derived using a Viewpoint Analysis (Burge, 2011). This method is particularly useful when stakeholders provide limited information. The result of the Viewpoint Analysis is a structured chart that describes the system functionality necessary to meet the operational requirements. In the first stage of the analysis a brainstorming session was employed to supplement the operational requirements. This phase encouraged considering aspects beyond operation, such as design, manufacturing, and maintenance (Dai and Aurisicchio, 2013). Subsequently the requirements were separated in functional and non-functional. The functional requirements were further separated into external (i.e. defining functionalities external to the system of interest) and internal. With this step the user interface and the interfaces to services and to the ablation kit were identified as specific functions. The functional requirements were then logically grouped and associated to the corresponding non-functional requirements as shown in the structured chart (Fig. 2). In particular the non-functional requirements affecting the whole system, such as cost and
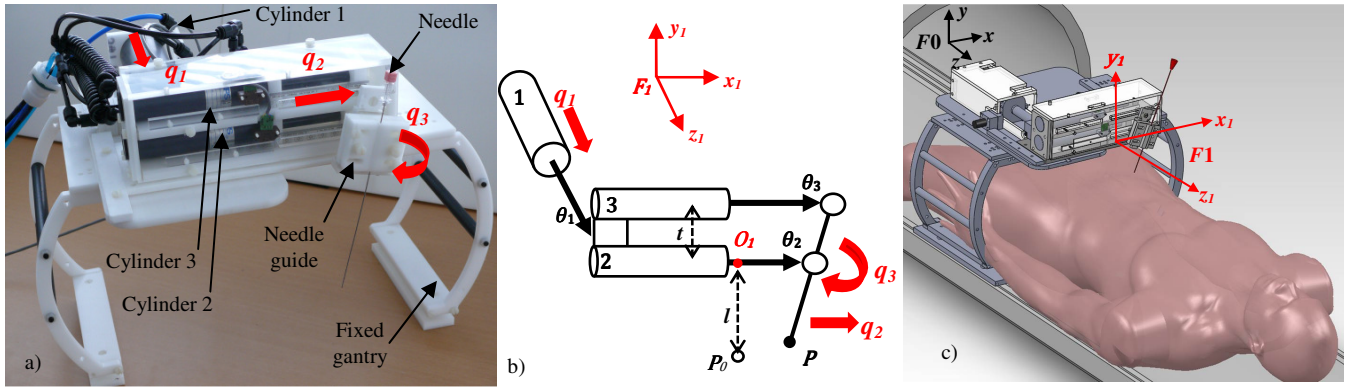
Fig. 3. Prototype of the needle positioner (a); kinematic diagram in isometric view (b): q_1, q_2, q_3 are the actuated movements of the needle guide, $\theta_1, \theta_2, \theta_3$ are the measured piston positions, cylinders are numbered form 1 to 3; CAD model (c): $F1$ and $F0$ are the coordinate frames of positioner and MR scanner.

MRI-compatibility are positioned at the top of the chart since they influence not just operation but they also affect design and manufacturing.

A Systemic Textual Analysis (Burge, 2004) was then employed to identify and interpret missing requirements. Integrating the requirements using a different method is particularly beneficial for new designs where the analysis cannot rely on the know-how accumulated over previous versions. Differently from the Viewpoint Analysis, the Systemic Textual Analysis focused only on operation related requirements (Dai and Aurisicchio, 2013) while other aspects, such as design, manufacturing and maintenance, were not directly considered. It must be noted however that the interface functions previously identified are included in the analysis and provide a more complete view of the system. Five performance requirements (*) were identified as missing and supplemented (Table 1). In particular the requirement for the robot workspace was defined based on the average size of the liver in adults (Kawamura, 1997). The requirement for the insertion direction was derived based on further consultations with clinicians and on the design of similar systems (Hata, Hashimoto and Tokuda, 2005).

As soon as a complete set of requirements becomes available their method of verification should be considered (Ward *et al*, 2002). This activity aims at making plans to answer the question "are we building the thing right?" (Alexander and Clarkson, 2000). Since this aspect was not explicitly covered by the previous methods an additional analysis was conducted. Candidate verification methods, acceptance criteria and model characteristics were then associated to each functional requirement (Table 2). This analysis allowed highlighting problematic requirements that cannot be verified and should therefore be reformulated. Additionally an indication of the effort and of the resources necessary for the verification was provided. While some requirements can be verified with simulations and models (e.g. FMEA, CAD), testing and prototypes are necessary in other cases. These different approaches should not be seen as mutually exclusive but should rather be combined (Ward *et al*, 2002). The requirements analysis highlights the need for a first prototype in order to verify the crucial aspects of the design. In particular the prototype should be capable of moving the needle in the MR scanner and of measuring its position. For this purpose a suitable control algorithm should

be designed and an effective localisation method should be employed to register and track the robot in the MR scanner. Additionally the system should allow verifying the needle insertion on the MR images and should make use of the standard coaxial needle. The design of the prototype is presented in the next section.

3. SYSTEM DESIGN

The prototype presented in this paper is intended to provide accurate point-to-point positioning of a needle guide inside a closed bore MR scanner and to assist the manual needle insertion outside the bore during phantom trials. The system consists of a remotely actuated positioner, a control unit containing control hardware and micro-controller, a graphical user interface on a host PC. This section describes the design of the prototype.

A. Robot Structure

The prototype was designed to be placed inside the MR scanner secured to the patient bed and consists of a fixed gantry and of a remotely actuated unit carrying a needle guide (Fig. 3.a). To ensure MRI compatibility plastic materials (Delrin, PTFE) were employed for the construction and double-acting plastic cylinders (IPS Inc.) were chosen for the actuation. In this first prototype the needle guide can translate along the x_1 and z_1 axes (movements q_1, q_2) and can only rotate around the z_1 axis (movement q_3) in the base frame $F1$ (Fig. 3.b). This configuration constrains the insertion direction on axial planes which is representative of only a subset of liver ablation procedures. However a modular structure was adopted in view of the introduction of a 4th DOF which would allow double-inclined insertions. Cylinder 1 is mounted orthogonally to the other two and moves them along the longitudinal axis of the MR scanner (1st DOF: q_1). Cylinder 2 and Cylinder 3 are arranged to provide needle translation (2nd DOF: q_2) when moved together and rotation (3rd DOF: q_3) when moved differentially. The needle guide is attached to pistons 2 and 3 with revolute joints. The relation between the joint coordinates (q_1, q_2, q_3) and the measured positions of the pistons $(\theta_1, \theta_2, \theta_3)$ is:

$$\begin{cases} q_1 = \theta_1 \\ q_2 = \theta_2 \\ q_3 = \tan^{-1}\left((\theta_3 - \theta_2)/t\right) \end{cases} \qquad (1)$$

The parameter t is the distance between Cylinder 2 and Cylinder 3. The base coordinate frame $F1$ was assigned with the axes z_1 and x_1 parallel to the prismatic joints q_1 and q_2 respectively. The fixed origin $O1$ of $F1$ is taken coincident to the lower revolute joint when all pistons are retracted. The needle tip P is located at a distance l from the origin $O1$. The relation between the generic position of P (q_1, q_2, q_3) in the frame $F1$, its initial position P_0 (0,0,0) and the joint coordinates is:

$$P(q_1, q_2, q_3) = T1(q_1) \cdot T_2^1 \cdot T2(q_2) \cdot T_3^2 \cdot T3(q_3) \cdot P_0 \qquad (2)$$

The terms $T1$, $T2$, $T3$ are 4×4 homogeneous transformation matrices, function of the joint coordinates. The misalignment between the joints q_2, q_3 and the axes x_1, z_1 caused by manufacturing and assembly tolerances is accounted for by the constant matrices T_2^1 and T_3^2 that are computed during calibration. The linear range of motion of the prismatic joints q_1 and q_2 is 80 mm. The angular range of motion of the revolute joint q_3 is +45° to -45° when q_2 is at mid-range. The limits on the workspace are dictated by the available space in the scanner bore which restricts the maximum size allowed for the actuators. Using the full range of motion allows targeting points within a volume corresponding to 60% of the liver size without having to manually reposition the gantry on the patient bed. For the LITT procedure the workspace is however considered acceptable since the location of the lesions within the liver is generally known from pre-interventional MR images. Consequently the gantry can be positioned accordingly on the patient bed at the start of the procedure (Fig. 3.c).

B. Actuation and Sensing

The size of the actuators was selected based on the space constraints in the MR scanner and on the external loads. The bore diameter of a 3T MR scanner is typically 60 cm to 70 cm (Siemens Verio) and the gantry should allow at least 25 cm clearance from the patient bed. Considering that Cylinder 2 and 3 are orthogonal to the axis of the bore their maximum extended length is 280 mm. This limits the cylinder stroke to about 100 mm which allows sufficient clearance with the scanner. The cylinder bore was chosen considering only inertial loads and friction forces (Table 3) since the prototype is not intended to come in contact with the patient. The pneumatic circuit (Fig. 4) features a proportional valve (Tecno Basic, Hoerbiger) supplying all cylinder front chambers at 2.3 bar while individual proportional valves are used to set the pressure within the range 0.3 bar to 2.3 bar in the cylinder back chambers. This ensures motion in both directions due to the different effective piston area in each cylinder chamber. The actuators behave like single acting cylinders with the advantage that a steel spring is not required, which would adversely affect the MRI compatibility of the system. This design choice reduces the number of supply lines from 6 to 4 resulting in space saving inside the MR scanner and requires fewer proportional valves than other similar devices (Song *et al*, 2010), (Melzer

Table 3   Actuators selection

Cylinder	Friction force [N]	Inertial load [N]	Calculated Bore [mm]	Stock bore [mm]
1	22	0.5	28	31.75
2	10	0.1	16	19
3	10	0.1	16	19

Nominal piston friction corresponds to 0.35 bar pressure. Inertial loads assume maximum acceleration 200 mm/s². The piston mass is 0.3 kg. A constant 2 bar pressure is considered acting in the cylinder front chamber. Stock bore is chosen immediately larger than calculated bore.
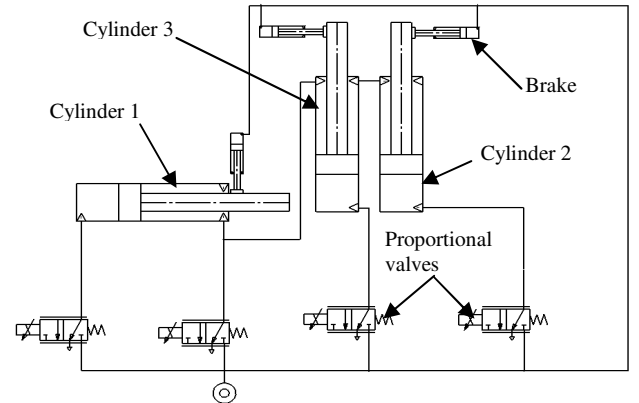

Fig. 4. Pneumatic circuit diagram.

et al, 2008). In spite of the common supply to the front chamber no mutual coupling between actuators was observed due to the slow movement of the pistons and the large flow rate the proportional valves can provide (ref. Section 6). The maximum pressure in the cylinders is constrained between 0.3 bar and 2.3 bar in order to enhance safety and to reduce air consumption. Non-metallic pneumatic brakes mounted orthogonally to each cylinder axis allow locking the pistons in position. Each brake consists of a miniature pneumatic cylinder with a silicone O-ring that acts as a return spring. Linear incremental encoders (EM1-250, US Digital) and quadrature counters (LS7366, LSI Computer Systems Inc.) are employed for position sensing (0.025 mm resolution). A homing procedure is employed at start-up during which all cylinders are retracted and the counters are reset.

A 9 m long shielded cable and 9 m long supply lines connect the positioner to the control unit, containing all electronic components and valves, outside the MR scanner room. An aluminium wave guide adapter with chassis-mount pi-section filters serves as interface for the cable on both sides of the panel to prevent EM noise from perturbing the MR environment. The microcontroller (mbed NXP LPC1768) in the control unit runs the real-time position control and the trajectory planning for each piston at 1 kHz. A Linux PC hosts a graphical user interface that communicates with the microcontroller and displays the MR images after each scan (Fig. 5). The user selects the target point graphically while the computed needle tip position is displayed on the MR image for verification (Fig. 6).

C. Calibration

The prototype was calibrated using independent measurements with an optical tracking system (Optotrak
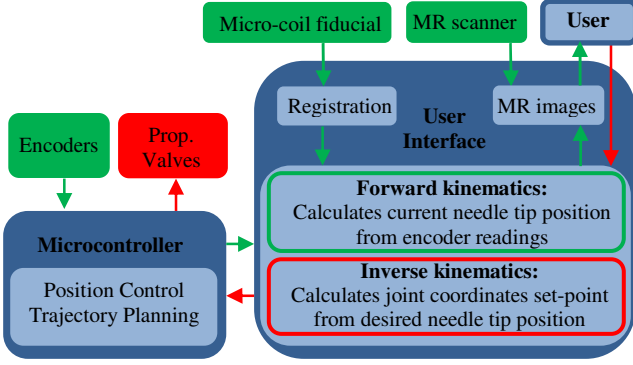
Fig. 5. Block-diagram of the system. Red arrows represent commands, green arrows represent feedback. The inner control loop runs on the microcontroller. The user closes the outer control loop using MR image feedback.
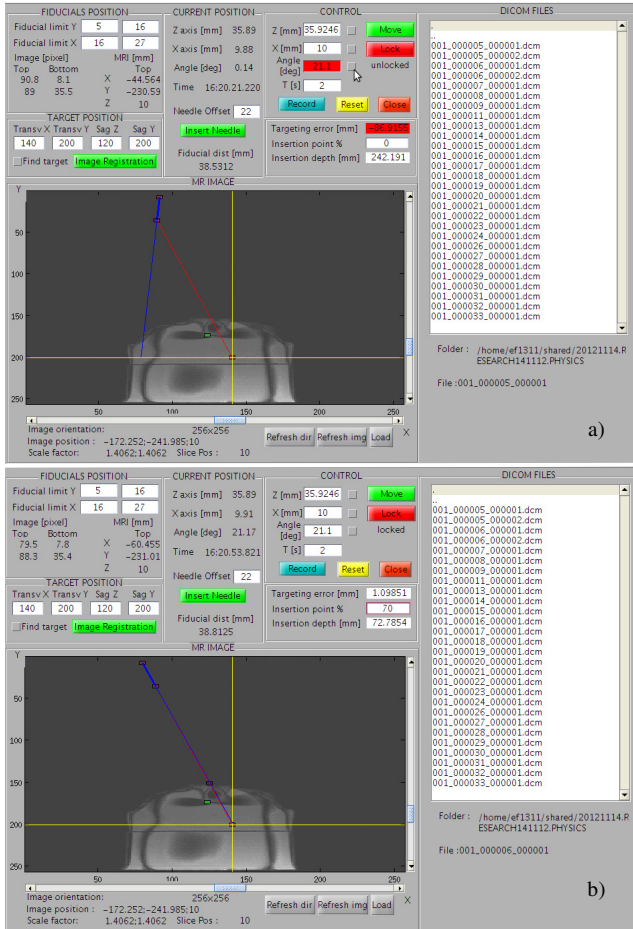

Fig. 6. Graphical user interface: target selection (a); needle alignment (b). Red line represents the insertion direction, blue line the needle axis, yellow lines intersect on the selected target.

Certus, NDI). An optical marker (Smart Marker, NDI) was mounted on an adapter 200 mm long attached to the needle guide, corresponding to the length of the coaxial needle. The identification of joint axes (Mooring, Roth and Driels, 1991) was employed: the actuated joints were moved one by one through their whole range of motion while the coordinates of the optical marker were measured with the tracking system. The constant matrices T^1_2 and T^2_3, the adapter length l and the distance t in (1), (2) were then estimated by least-squares.

4. CONTROLLER DESIGN

An improved SMC scheme based on SMC theory (Slotine and Li, 1991) has been designed to achieve accurate position control in spite of the high friction. Similarly to (Chang, Hwang and Hsieh, 2002) the control law employs nested boundary layers. However in this control scheme the boundary layers are defined by two saturation functions that instead of acting individually compensate friction concurrently. The control design is based on the reduced-order model of the piston's dynamics:

$$A \times U - A' \times P_2 = m\ddot{x} + \gamma\dot{x} + F_a \operatorname{sign}(\dot{x}) \qquad (3)$$

The terms m, A, A', P_2 are respectively the mass of the piston, the effective piston areas and the constant pressure in the front cylinder chamber. The terms γ and F_a are the actual unknown values of viscous and Coulomb friction. Similarly to (Yang $et\ al$, 2011b) the much faster dynamics of the proportional valve and the delay introduced by the pipes are not considered in the design. To construct the control law U the positive definite Lyapunov function $V = 1/2S^2$ is defined, where S is a function of the piston position x and velocity $\dot{x}$ and of their prescribed values (Slotine and Li, 1991):

$$S = \lambda(x_{SET} - x) + (\dot{x}_{SET} - \dot{x}) \qquad (4)$$

The parameter $\lambda = 12.5$ Hz was chosen based on the largest un-modelled delay as indicated in (Slotine and Li, 1991). The delay (approximately 28 ms) was measured from the step response of the proportional valve connected to a pressure sensor (MPX4520GDP, 1 ms response time) with a 9 m pipe. The piston velocity $\dot{x}$ is calculated by discrete differentiation of the measured position x followed by first order low pass Butterworth filter. The corner frequency of the filter was set to 120 Hz considering that the unfiltered velocity shows high spectral density only below 50 Hz.

The control law ensures a stable error dynamics if $\dot{V} = S\dot{S} \le 0$. The improved control law proposed here is:

$$U = u_{eq} + u_1 + u_2 \qquad (5)$$

The term u_{eq} keeps the system on the sliding surface $S = 0$:

$$u_{eq} = \frac{A'\,P_2}{A} + \frac{\dot{x}\hat{\gamma}}{A} + \frac{m\ddot{x}_{SET}}{A} + \frac{m(\dot{x}_{SET} - \dot{x})\lambda}{A} + \frac{\hat{F}_a \operatorname{sign}(\dot{x})}{A} \qquad (6)$$

The terms $\hat{\gamma}$ and $\hat{F}_a$ are the nominal values of viscous and static friction provided by the cylinder manufacturer. The remaining terms in (5) are saturation functions and compensate for model uncertainty:

$$u_1 = a \times \operatorname{sat}(S/b) = \begin{cases} a \times \operatorname{sign}(S/b) & |S| \ge b \\ a \times S/b & |S| < b \end{cases}$$

$$u_2 = \begin{cases} c \times \operatorname{sat}(S/e) & |S| < b \\ 0 & |S| \ge b \end{cases} \qquad (7)$$

Assuming known the bounds $|\hat{F}_a - F_a| \le F$ and $|\hat{\gamma} - \gamma| \le \Gamma$ the positive parameters a and c are chosen as:

$$a = F/A + \Gamma |\dot{x}|/A + \eta$$
$$c = F/A + \Gamma |\dot{x}|/A \qquad (8)$$

The boundary layer thickness b and e ($e < b$) and the positive constant η are empirically tuned. To verify the

stability of the control scheme (5) the derivative $\dot{V}$ is computed differentiating (4) and substituting (3) and (5):

$$\dot{V} = \frac{S}{m}\left(\left(F_a - \hat{F}_a\right)\text{sign}(\dot{x}) + (\gamma - \hat{\gamma})\dot{x}\right) - \frac{SA}{m}\left(u_1 + u_2\right)$$
$$= S\left(\Delta f - Au_1 - Au_2\right)/m \tag{9}$$

The term Δf in (9) represents the maximum variation of the friction forces. Substituting (7) and (8) we rewrite (9) as:

$$\dot{V} \leq \begin{cases} -\eta\,|S|\,\dfrac{A}{m} < 0; & |S| \gtrsim b \\[2mm] -\left(\dfrac{F}{m} + \dfrac{\Gamma\,|\dot{x}|}{m} + \dfrac{\eta A}{m}\right)\left(\dfrac{S^2}{b}\right) < 0; & b > |S| > e \\[2mm] S/m\left(\Delta f - (F + \Gamma\,|\dot{x}|)\left(\dfrac{S}{b} + \dfrac{S}{e}\right) - \dfrac{\eta A S}{b}\right); & |S| \lesssim e \end{cases} \tag{10}$$

Since $\dot{V} \leq 0$ for $|S| > e$ the system is globally uniformly bounded with the control law (5). For $|S| \geq b$ the control scheme is equivalent to a standard SMC. It is apparent that a larger η produces a more responsive control action and a faster convergence to the bound. Adding u_2 inside the boundary layer makes $\dot{V}$ negative definite for $b > |S| > e$ which leads to higher accuracy with the same tuning of η and b.

For comparison purposes the following baseline control law is considered as an alternative to (5):

$$U' = u_{eq} + u'_1$$
$$u'_1 = a \times \text{sat}\left(S/b'\right) \tag{11}$$
$$b' = e$$

In this case the system is also bounded by $|S| = e$ however a smaller value of η should be chosen to avoid overshoot and oscillations. This can also results in less responsive control. In the proposed control scheme (5) instead the contribution of the term η decreases linearly for $|S| < b$. At the same time u_2 balances completely the friction forces for $b > |S| > e$. Consequently a fast convergence to $|S| \leq b$, desirable for tracking tasks, is followed by a more gentle convergence to $|S| = e$, which is desirable for point-to-point positioning tasks.

5. ROBOT LOCALISATION

The accurate registration of the base frame $F1$ of the needle positioner in the MR scanner is essential in order to achieve the desired targeting accuracy. This procedure involves independently measuring the position of the robot in the coordinate frame $F0$ of the scanner. Fiducial markers of different types are typically employed for this purpose (Rea *et al*, 2008) together with various localisation techniques. Fiducial markers can be grouped in three main categories. Active micro-coil fiducials provide a signal to a dedicated channel of the MR scanner by means of a connecting wire (Dumoulin, Souza, Darrow, 1993). The main advantage of this approach is that the signal is highly localised and therefore less sensitive to background noise. However the connecting wire adds complexity to the design and experiences heating as a consequence of the electromagnetic coupling (Konings *et al*, 2000) which poses a safety hazard. Semi-active fiducials typically consist of a
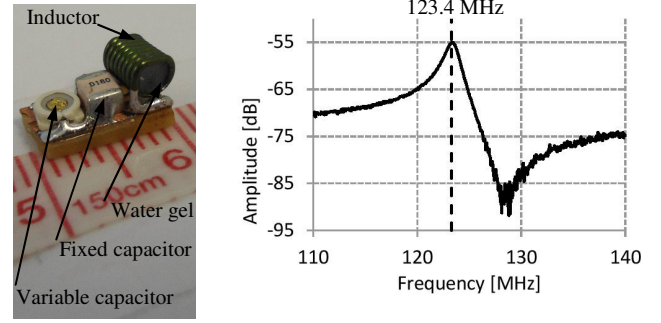

Fig. 7. Wireless micro-coil fiducial (left) and frequency response (right).

resonant circuit inductively coupled to a receiver coil in the MR scanner (Burl, Coutts, Young, 1996). Differently from active fiducials a wired connection to the scanner is not required which simplifies the design but makes this approach more sensitive to background noise. In spite of the moderate heating that can occur due to electromagnetic coupling these markers are considered relatively safe if they don't come into direct contact with the patient (Garnov *et al*, 2011). Finally passive markers typically consist of capsules containing high-contrast material that appears as a bright region on the MR images. Passive markers offer the simplest solution from a design prospective and are comparatively inexpensive. Additionally they do not experience heating and are therefore completely safe. Passive markers are typically localised using image processing methods such as template matching (de Oliveira *et al*, 2008). These methods are applicable in principle to all types of markers and can be used with standard imaging sequences. Consequently this approach is completely portable and can be employed as is on different types of scanners. The main drawback is the rather long time associated to 2D image reconstruction of many standard imaging sequences (McRobbie *et al*, 2003). Active and semi-active fiducials can also be localised using special imaging sequences that employ orthogonal one-dimensional (1D) projections of the marker signal. This method is considerably faster than image processing and offers high resolution.

The prototype presented here makes use of semi-active markers localised using a tracking algorithm that employs 1D projections (Galassi *et al*, 2014). The method involves acquiring a set of 1D projections through excitation of the whole imaging volume. For this purpose a modified Gradient Echo sequence (GRE, TR = 5.6 ms, TE = 3.5 ms, FOV = 300) is used. The peaks generated by each marker are then detected for each projection and the marker positions are computed in three dimensions with sub-millimetre accuracy. The fiducials consist of wireless micro-coils tuned at the Larmor frequency corresponding to the field strength of the MR scanner (123.4 MHz at 2.9 T for Siemens Verio). Previous designs typically employed fixed capacitors in parallel with an inductor constructed hand-winding a copper wire around a cylindrical former while keeping small gaps between the turns to allow fine tuning (Rea *et al*, 2008). In this work tuneable micro-coils were constructed using a non-magnetic air core inductor (Coil Craft) filled with water gel (vinyl plastisol gel, Spenco Healthcare Ltd) and a ceramic trimmer capacitor in parallel with a fixed capacitor (Passive Plus Inc.). The advantages of this approach are higher repeatability and shorter manufacturing time thanks to the use of standard components. Additionally the trimmer

capacitor allows easily tuning the micro-coils and potentially reusing them for different field strengths. The overall micro-coil assembly measures 10 mm in length and 5 mm in width and height (Fig. 7). Instead of using markers mounted on a rigid frame for registration (Seifabadi *et al*, 2012) three fiducials are attached directly to the needle guide This approach reduces registration errors since it locates the needle guide directly and is therefore insensitive to the manufacturing tolerances of the supporting structure.

6. EXPERIMENTAL RESULTS

Experimental tests were conducted to verify the MRI compatibility of the system, to evaluate the performance of the controller and to assess the accuracy of the needle positioner in the MR scanner.

A. MRI Compatibility

The MRI compatibility of the prototype was tested in a 3T MR scanner (Siemens Verio). The prototype was placed on the patient bed above a cylindrical phantom (Nickel Sulphate solution) and the needle guide was aligned with the scanner isocenter (Fig. 8). The imaging sequences used were a Turbo Spin Echo (TSE, TR = 3000 ms, TE = 12 ms, FA = 180°, FOV = 300 x 300, Slice Thickness = 8 mm) and a True
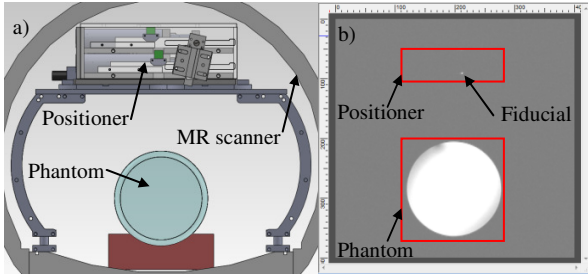

Fig. 8. CAD model of the positioner in the MR scanner (a); corresponding axial MR image with the positioner powered on (b).
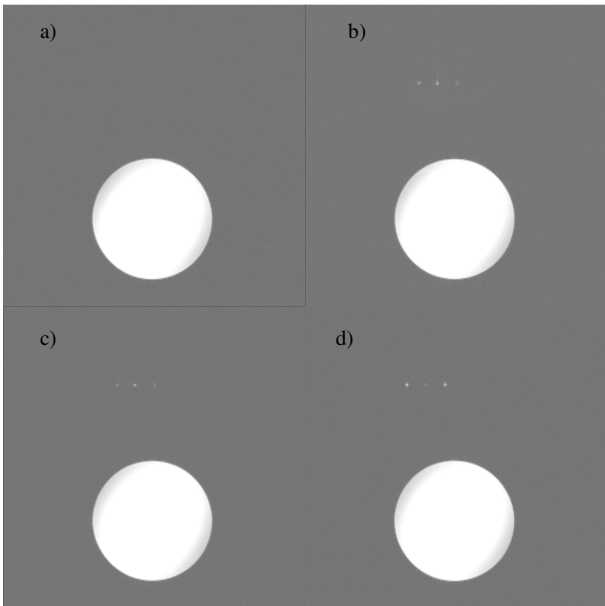

Fig. 9. MR images (TrueFISP): Phantom (a); Power off (b); Power on (c); Movement (d). Fiducials indicate the presence of the positioner.

Table 4   MRI Compatibility of the Needle Positioner

Setup	TrueFISP		TSE	
	SNR	%Variation	SNR	%Variation
Phantom (reference)	115.5	-	546	-
Power off	115.1	-0.4%	536	-1.8%
Power on	115.2	-0.3%	531	-2.7%
Movement	114.2	-1.1%	530	-2.9%

Variations in SNR calculated for test in 3T MR scanner.

fast imaging with steady-state precession (TrueFISP, TR = 4.4 ms, TE = 2.2 ms, FA = 44°, FOV = 400 x 400, Slice Thickness = 8 mm) in conjunction with the scanner Body coil. In total four sets of images were acquired considering first the positioner disconnected from the control unit, then powered on but not moving, and finally with each piston executing a sinusoidal trajectory. The fourth condition used for comparison refers to the phantom alone. The prototype did not produce visible artefacts within the region of interest with both TrueFISP (Fig. 9) and TSE sequences. The variation in signal-to-noise ratio (SNR) compared to the phantom alone calculated according to (NEMA Standard Publication, 2008) remained below 3 % for all test scenarios (Table 4). Additionally no interference in the measured position was detected as a result of the MR environment.

B. Controller Performance

The advantages of the improved controller (5) over the baseline scheme (11) are highlighted with step tests and tracking tests on Cylinder 1 alone mounted horizontally as in the prototype. Tests were also performed using a 2.5 kg mass to evaluate the robustness of the controllers. Both control schemes are equally simple to implement on the microcontroller and both rely on the same assumption of bounded variation of the friction forces (ref. Section 4). Scheme (11) requires manually tuning 2 parameters (b, η) while guidelines exists for tuning the parameter λ. The controller (5) requires tuning one additional parameter ($e < b$) which however can be chosen from the step response of the baseline scheme (11). The procedure for tuning the parameter e is as follows: 1) increase the value of b until the overshoot in the step response disappears; 2) choose a value of e larger than the steady-state error; 3) set the values found for b and e in (5); 4) further adjust e to reduce either the overshoot or the steady-state error. The numeric values of controller and model parameters are listed in Table 5. The value b'=0.01 was used in (11) for all tests in order to present a meaningful comparison since choosing b'=e resulted in excessive chattering.

Table 5   Controller and Model Parameters for Cylinder 1

Parameters	λ	$\hat{F}_a/A$	F/A	$\hat{\gamma}$	Γ	b	e	η
Value	12.5	0.35	0.35	20	20	0.1	0.004	0.75
unit	Hz	bar		Ns/m			m/s	bar

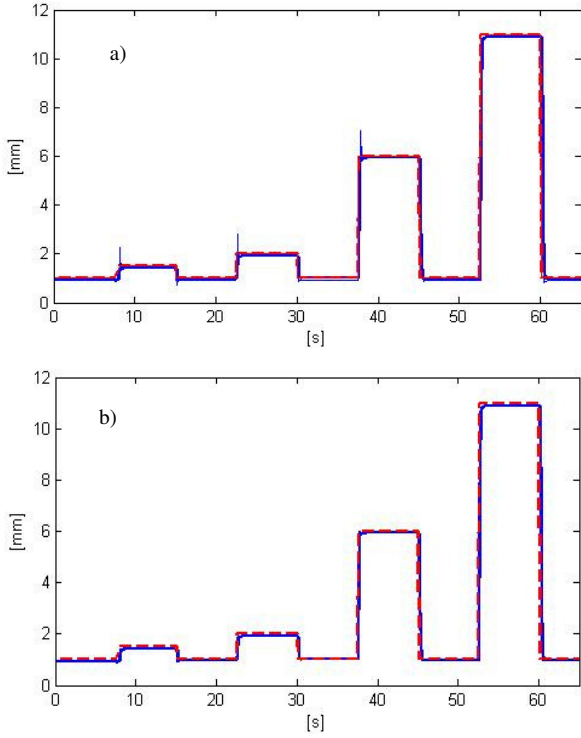Parameters b, e, η are manually tuned; λ is chosen as per Section 4.

Fig. 10. Step response for Cylinder 1 without additional mass for: (a) baseline SMC scheme (11); (b) improved SMC scheme (5). Red dashed line represents the set-point; blue solid line the measured position.
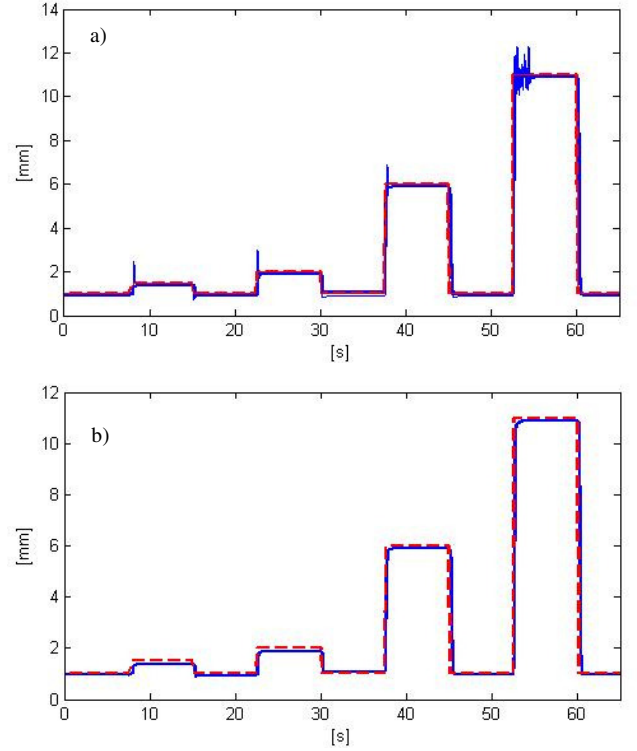

Fig. 11. Step response for Cylinder 1 with 2.5 kg additional mass for: (a) baseline SMC scheme (11); (b) improved SMC scheme (5). Red dashed line represents the set-point; blue solid line the measured position.

Step tests with amplitudes of 0.5 mm, 1 mm, 5 mm and, 10 mm were repeated 10 times for both control schemes (5) and (11). The step response for both controllers without additional mass is depicted in Fig. 10 while Fig. 11 refers to the test with additional mass. Compared to the baseline scheme (11), the improved controller (5) achieved noticeably lower overshoot and equivalent steady-state error in all test conditions (Table 6) and shorter settling time in the test with the 2.5 kg mass.

The tracking performance was evaluated with a periodic constant-jerk polynomial trajectory (20 mm peak-to-peak amplitude, 3s period). The piston position for the test without additional mass is depicted in Fig. 12. Compared to the baseline scheme (11), the improved controller (5) achieved smaller root-mean-square error (RMSE) and smaller tracking error (Table 7). The corresponding control input is depicted in Fig. 13. The baseline scheme (11) shows a more intense

control action where the control input frequently hits the upper and lower limits defined in Section 3. This is due to the narrower boundary layer ($b' < b$) which reduces the linear region of the saturation function (ref. Section 4) and results in a more aggressive control. Consequently the piston trajectory is less smooth compared to control scheme (5). Similar results were obtained in the test with the additional mass. In conclusion the improved controller (5) performed better in both step test and tracking tests and was therefore deemed more suitable for the needle positioner.

Finally the accuracy of all three actuated axes was assessed with the control scheme (5). The position error for all three actuated axes was measured over 100 point-to-point movements with amplitudes varying from 0.3 mm to 20 mm in both directions of motion starting from the retracted position. The maximum steady-state error for all axes was below 0.16 mm and the highest mean absolute error was below 0.1 mm. The dynamic response was evaluated actuating the pistons first individually and then

Table 6   Step Response for Cylinder 1

Controller	$U = u_{eq} + u_1 + u_2$ Improved Scheme (5)		$U' = u_{eq} + u_1'$ Baseline Scheme (11)	
Load [kg]	0	2.5	0	2.5
Overshoot [mm]	0.01	0	1.15	1.63
Settling time [s]	0.66	0.77	0.64	1.40
Steady state error [mm]	0.10	0.14	0.10	0.13

Values are the maximum over a set of 4 step responses with amplitudes 0.5 mm, 1 mm, 5 mm and 10 mm each repeated 10 times.

Table 7   Tracking Error for Cylinder 1

Controller	$U = u_{eq} + u_1 + u_2$ Improved Scheme (5)		$U' = u_{eq} + u_1'$ Baseline Scheme (11)	
Load [kg]	0	2.5	0	2.5
Maximum error [mm]	1.74	1.45	1.97	2.15
RMSE [mm]	0.45	0.53	0.69	0.78

Values refer to a periodic polynomial trajectory with 3 s period and 20 mm peak-to-peak amplitude.
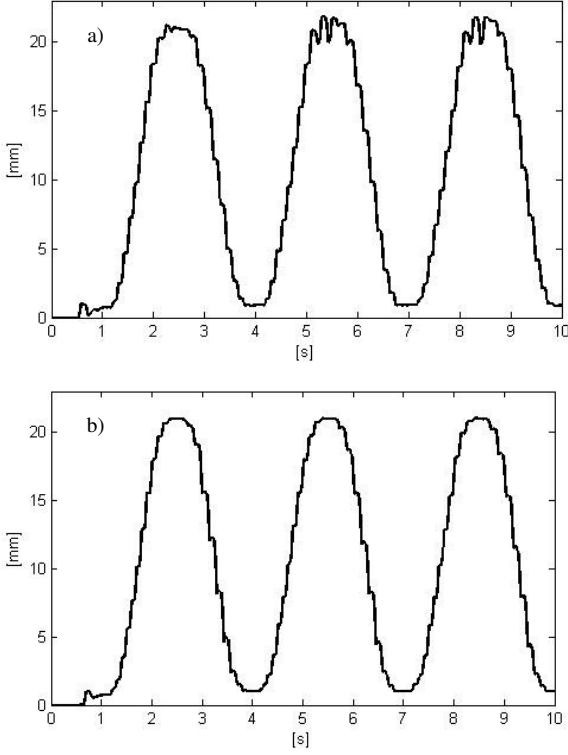
Fig. 12. Piston trajectory for Cylinder 1 without additional mass: (a) baseline SMC scheme (11); (b) improved SMC scheme (5).

Fig. 13. Control input for Cylinder 1: (a) baseline SMC scheme (11); (b) improved SMC scheme (5).

simultaneously. At the same time the pressure in the front cylinder chambers was monitored with a sensor (MPX4520GDP, 35 mbar accuracy) on the common supply line. The pistons followed smoothly the prescribed constant-jerk trajectories (up to 40 mm executed in 2 s). Moreover no coupling between actuators and no noticeable variation in the measured pressure was detected in spite of the common supply to the front cylinder chambers (Fig. 14).

C. Robot Accuracy

The accuracy of the positioner was assessed in the MR scanner over 20 target points within the workspace (Fig. 15). A micro-coil fiducial was placed on an adapter 200 mm long attached to the needle guide. This setup simulates a fully inserted needle and amplifies position errors of θ_2 and θ_3 by a factor 5, corresponding to the ratio between adapter length l and distance t (1). The coordinates of the micro-coil in the reference frame $F0$ of the MR scanner were calculated using the tracking algorithm described in (Galassi *et al*, 2014). Initially the reference frame $F1$ was automatically registered with respect to the scanner frame $F0$ computing the position of 3 points with (2) and measuring the corresponding position of the micro-coil fiducial with the tracking algorithm. Subsequently the desired marker position in the base frame $F1$ was calculated with (2) from the set values of the joint coordinates and then transformed in the scanner frame $F0$. The position of the 20 points was measured three times over two hours, which corresponds to the average duration of a LITT procedure. The deviation was calculated as distance between the desired and the measured position. The mean position error for each dataset is between 1mm and 1.5mm while the maximum error is below 2.1 mm (Table 8).
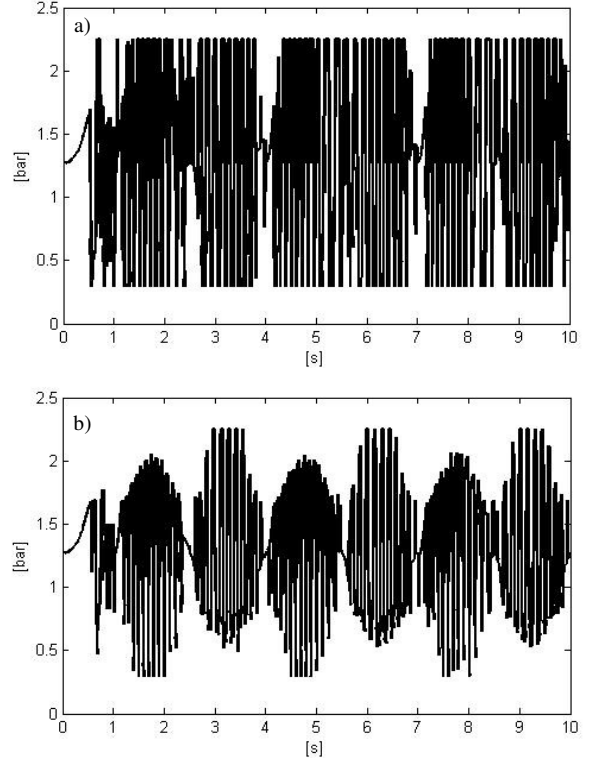
A preliminary phantom study was conducted to evaluate the targeting accuracy of the positioner in the MR scanner. A water-phantom with plastic circular features (diameters from 6 mm to 12 mm) visible on the MR images was used for the experiment. The phantom was positioned horizontally on the patient bed and aligned with the scanner isocenter. After the automatic registration in the MR scanner the graphical user interface was employed to plan the needle insertion. For each target: 1) an initial MR image of the phantom was acquired; 2) the operator graphically selected the target on the MR image; 3) the software calculated the movement of each
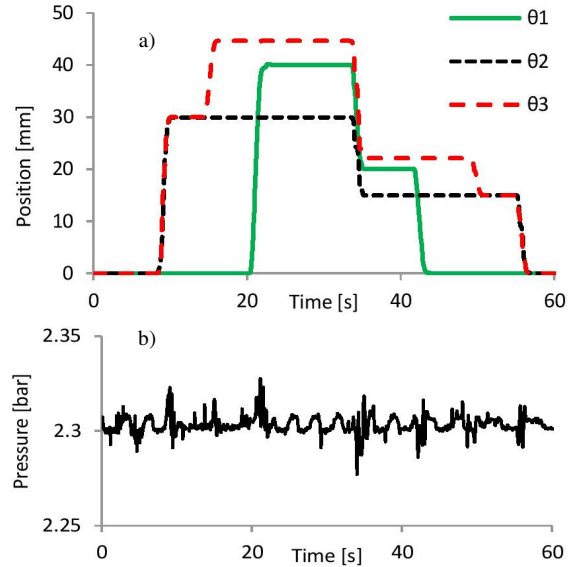

Fig. 14. Constant jerk trajectories for each piston ($\theta_1, \theta_2, \theta_3$) with 2 s set for the movements (a). Pressure in the cylinders' front chambers (b).
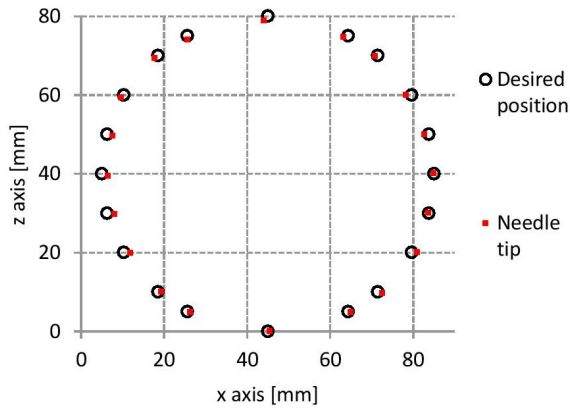
Fig. 15. Needle-tip desired and actual position on the x_1-z_1 plane in the base frame $F1$ of the positioner.

Table 8 Accuracy in 3T MR Scanner

	Dataset 1	Dataset 2	Dataset 3
Mean error [mm]	1.32	1.36	1.21
Maximum error [mm]	2.07	2.08	2.06

Needle-tip position error for 3 datasets over 2 hours in 3T MR scanner.

joint; 4) the positioner automatically aligned the needle guide with the target; 5) the patient bed was moved out of the bore and a plastic needle was manually inserted using the needle guide; 6) the patient bed was moved back in the bore and a second MR image was aquired to verify the needle position. The procedure was repeated for eight insertions on four different targets. The in-plane targeting error was computed as distance between the center of the circular feature and the center of the needle artefact using the 3D Slicer software package (3D Slicer, 2004). The mean error was 1.8 mm with a maximum of 3.2 mm. Coronoal images of four different test conditions are depticed in Fig. 16.

7. CONCLUSIONS

The first prototype of a MRI-compatible needle positioner with low pressure pneumatic actuation and long supply lines intended for MRI-guided LITT of the liver has been presented. The design of the system was based on a detailed analysis of the requirements. The prototype can operate inside a high-field MR scanner while being remotely actuated form the control room. The MRI compatibility of the prototype was investigated showing minimum alterations to the MR images. Sufficient point-to-point accuracy was achieved with an improved SMC scheme. Compared to a standard SMC design the controller allowed achieving smaller overshoot and shorter settling time in the step response and better tracking accuracy. Experiments in the MR scanner suggest that the accuracy of the system would be sufficient for clinical use. Further work will include the development of a second prototype with an additional angular DOF to allow inclined needle insertions on both sagittal and transversal planes. We also aim at further enhancing the accuracy of the system in order to offer clear advantages over the manual procedure. Finally the potential time saving associated with the use of the needle positioner
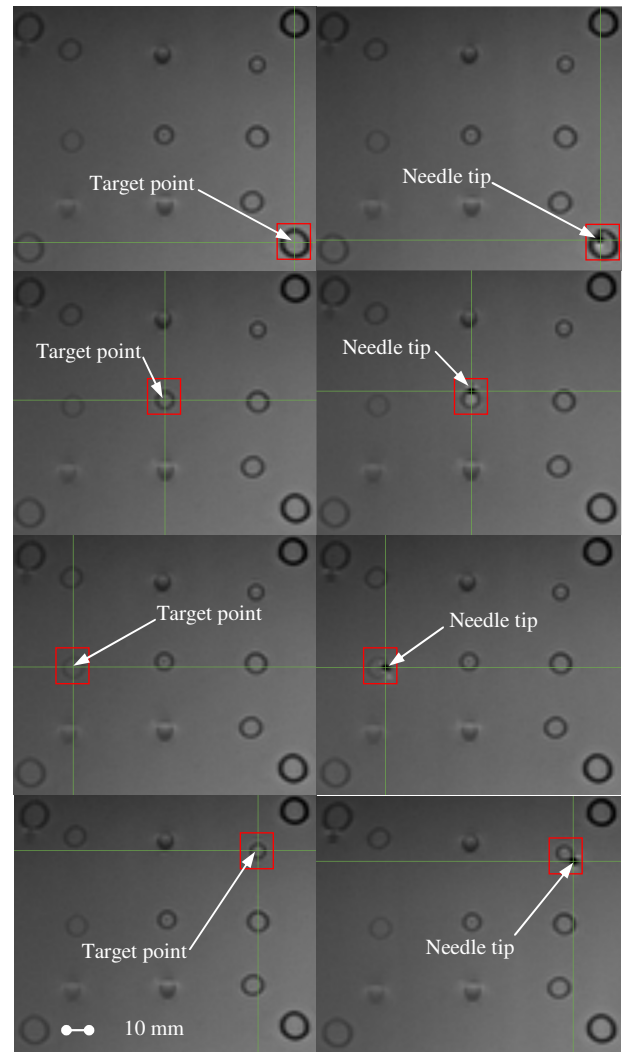

Fig. 16. Preliminaty phantom study: target position (left); needle tip position (right).

compared to manual procedures will be evaluated with experiments.

REFERENCES

3-D Slicer (2004) [online], http://www.slicer.org, [Accessed 01/10/14]

Alexander K., Clarkson P.J. (2000),'Good design practice for medical devices and equipment, Part II: Design for validation,' Journal Medical Engineering Technology, 2000 Mar-Apr; 24(2):53-62.

Yang, B.; U-Xuan Tan; McMillan, A.; Gullapalli, R. and Desai, J.P. (2011a) 'Design and implementation of a pneumatically-actuated robot for breast biopsy under continuous MRI,' in Proceedings of the *IEEE International Conference on Robotics and Automation (ICRA), 2011,* Vol., no., pp.674,679.

Yang, B.; U-Xuan Tan; McMillan, A.B.; Gullapalli, R. and Desai, J.P. (2011b) 'Design and Control of a 1-DOF MRI-Compatible Pneumatically Actuated Robot With Long Transmission Lines,' *Transactions on Mechatronics, IEEE/ASME*, Vol.16, no.6, pp.1040-1048.

Burge, S. (2004), 'Systemic Textual Analysis (STA),' [onine] Burge Hughes Walsh, available from: www.burgehugheswalsh.co.uk. [Accessed 05/10/2014].

Burge, S. (2007) 'Stakeholder Influence Map (SIM),' [onine] Burge Hughes Walsh, available from: www.burgehugheswalsh.co.uk. [Accessed 05/10/2014].

Burge, S. (2011) 'Viewpoint Analysis,' [onine] Burge Hughes Walsh, available from: www.burgehugheswalsh.co.uk. [Accessed 05/10/2014].

Burl, M.; Coutts, G.A.; Young, I.R. (1996) 'Tuned fiducial markers to identify body locations with minimal perturbation of tissue magnetization,' Magn Reson Med 36(3):491–493

Chang, W. ; Hwang, R. ; Hsieh, J. (2002) 'Application of an auto-tuning neuron to sliding mode control,' *IEEE Transactions on Systems, Man, and Cybernetics, Part C: Applications and Reviews* , vol.32, no.4, pp.517-522.

Dai, W.; Aurisicchio, M. (2013),'An empirical investigation of requirements evolution in an industrial project,' in Proceedings of the *International Conference on Engineering Design (ICED) 2013*, Vol., no., pp.369-378.

de Oliveira, A.; Rauschenberg, J.; Beyersdorff, D.; Semmler, W.; Bock, M. (2008),'Automatic passive tracking of an endorectal prostate biopsy device using phase-only cross-correlation,' Magn Reson Med 59(5):1043–1050

Dick, E.A.; Taylor-Robinson ,S.D.; Thomas, H.C. and Gedroyc, W.M. (2002) 'Ablative therapy for liver tumours,' *Gut*, Vol. 50, pp.733-739.

Dumoulin, C.L.; Souza, S.P.; Darrow, R.D. (1993), 'Real-Time position monitoring of invasive devices using magnetic-resonance,' Magn Reson Med 29(3):411–415.

Galassi, F.; Brujic, D.; Rea, M.; Lambert, N.; Desouza, N.; Ristic, M. (2014) 'Fast and accurate localization of multiple RF markers for tracking in MRI-guided interventions,' Magnetic Resonance Materials in Physics, [online] http://link.springer.com/article/10.1007%2Fs10334-014-0446-3# , (Accessed 10/10/14).

Garnov, N.; Thormer, G.; Trampel, R.; Grunder, W.; Kahn, T.; Moche, M.; Busse, H. (2011), 'Suitability of miniature inductively coupled RF coils as MR-visible markers for clinical purposes,' Med Phys 38(11):6327–6335

Gedroyc, W.M. (2005) 'Magnetic resonance guidance of thermal ablation,' *Topics in Magnetic Resonance Imaging,* Vol. 16, pp.339-353.

Gough-Palmer, A.L. and Gedroyc, W.M. (2008) 'Laser ablation of hepatocellular carcinoma--a review,' *World Journal of Gastroenterology,* Vol. 14, pp.7170-4.

Kawamura, D. M. (1997), *Diagnostic Medical Sonography: Abdomen and Superficial Structures*. Philadelphia: Lippincott Williams & Wilkins.

Konings, M.K.; Bartels, L.W.; Smits, H.F.; Bakker, C.J. (2000), 'Heating around intravascular guidewires by resonating RF waves,' J. Magn. Reson. Imaging 12, 79–85 (2000).

McRobbie, D. W.; Moore, E. A; Graves, M. J.;Prince, M. R. (2003), *MRI – From Picture to Proton: What you set is what you get: basic image optimization*, Cambridge University Press, 2003.

Melzer, A.; Gutmann, B.; Remmele, T.; Wolf, R.; Lukoscheck, A.; Bock, M.; Bardenheuer, H. and Fischer, H. (2008) 'INNOMOTION for Percutaneous Image-Guided Interventions,' *IEEE Engineering in Medicine and Biology Magazine,* Vol.27, no.3, pp.66-73.

Mooring, B. W.; Roth, Z. S.; Driels, M. R. (1991), *Fundamentals of Manipulator Calibration*. New York: Wiley Interscience, p.165-191.

Hata, N.;Hashimoto, R.; Tokuda, J (2005), 'Needle guiding robot for MR-guided microwave thermotherapy of liver tumor using motorized remote-center-of-motion constraint,' in Proceedings of the *IEEE International Conference on Robotics and Automation (ICRA), 2005,* Vol., no., pp.1652-1656.

NEMA Standard Publication (2008), *Determination of signal-to-noise ratio (SNR) in diagnostic magnetic resonance imaging*, 2008, NEMA MS 1-2008.

Rea, M.; McRobbie, D.; Elhawary, H.; Tse, Z.; Lamperth, M.;Young, I. (2008), 'Sub-pixel localisation of passive micro-coil fiducial markers in interventional MRI,' *Magnetic Resonance Materials in Physics,*Vol. 22, no. 2, pp 71-76.

Sang-Eun Song; Cho, N.B.; Fischer, G.; Hata, N.; Tempany, C.; Fichtinger, G. and Iordachita, I. (2010) ,'Development of a pneumatic robot for MRI-guided transperineal prostate biopsy and brachytherapy: New approaches,' in Proceedings of the *IEEE International Conference on Robotics and Automation (ICRA), 2010* , Vol., no., pp.2580-2585.

Seifabadi, R.; Cho, N.B.; Song, S.E.; Tokuda, J.; Hata, N.; Tempany, C.M.; Fichtinger, G.; Iordachita, I. (2012), 'Accuracy study of a MRI-guided robotic system for prostate biopsy,' *Int J Med Robot.*

Slotine, J.-J; Li, W. (1991), *Applied Nonlinear Control*, Englewood Cliffs, New Jersey, Prentice-Hall.

Vogl, T.J.; Straub, R.; Eichler, .K; Woitaschek, .D; Mack, M.G., (1995) 'Malignant liver tumors treated with MR imaging-guided laser-induced thermotherapy: technique and prospective results,' *Radiology*, Vol. 196, pp.257-265.

Ward, K..; Clarkson, P. J.; Bishop D.; Fox, S., 1999, 'Good design practice for medical devices and equipment- design verification,' Workbook (Cambridge, UK: Cambridge University Engineering Department, Cambridge University)

WHO: Medical device regulations: global overview and guiding principles. vol. 24, no. 3. Geneva: WHO, 2003.